J|A|C|S
ARTICLES
Published on Web 05/19/2006

Insights on Charge Transfer Doping and Intrinsic Phonon Line Shape of Carbon Nanotubes by Simple Polymer Adsorption

Moonsub Shim,*,† Taner Ozel,‡ Anshu Gaur,† and Congjun Wang†

Department of Materials Science and Engineering and Department of Physics, University of Illinois at Urbana-Champaign, Urbana, Illinois 61801

Received December 16, 2005; E-mail: mshim@uiuc.edu

Abstract: Doping of individual single-walled carbon nanotubes via noncovalent adsorption of polyethylenimine which converts p-type semiconducting nanotubes into n-type is examined by micro-Raman studies. Distinctively different responses are observed in metallic and in semiconducting nanotubes. Very little or no changes in the radial breathing and the disorder modes are observed upon polymer adsorption on semiconducting carbon nanotubes indicating noncovalent nature of this process. Tangential G-band spectral downshift of up to $\sim$10 cm^{-1} without line broadening is observed for semiconducting tubes suggesting similar magnitude of electron transfer as commonly observed in electrochemical doping with alkali metals. Strong diameter dependence is also observed and can be explained by thermal ionization of charge carriers with activation barrier that scales as the energy gap of the semiconducting nanotubes. In contrast, metallic nanotubes exhibit very different behavior with significant line broadening of the G-band and concurrent enhancement of the disorder mode. In certain cases, initially symmetric Lorentzian line shapes of the G-band features with narrow line widths similar to semiconducting tubes are converted to a broad, asymmetric Breit−Wigner−Fano line shape. Implications on the effects of electron injection and the local chemical environment on the intrinsic line shape of isolated carbon nanotubes are discussed.

Introduction

Inherent to the nanometer length scale is the large surface-to-volume ratio. While spatial confinement leads to many interesting and potentially useful properties for breakthrough technologies,[1] large surface areas can impose severe difficulties in understanding and therefore in the ability to control materials' properties. For example, doping via impurity atoms has been and continues to be a challenge for nanoscale semiconductor materials[2] because of impurities being easily annealed out to the surface where dangling bonds/trap states can render doping ineffective. Often highly exposed electronic wave functions of nanoscale materials lead to extreme sensitivities but large fluctuations in responses even to minute changes in the ambient surrounding can give rise to potential ambiguities in the interpretation of experimental results.[3] Although single-walled carbon nanotubes (SWNTs) possess many desirable properties such as high carrier mobilities,[4] high current carrying capacities,[5] and mechanical robustness,[6] their all surface atom makeup represents the ultimate challenge in understanding of the influence of extrinsic factors to the intrinsic properties of nanoscale materials. Such an understanding is necessary for the ability to control materials' properties especially at the nanometer dimensions.

With respect to semiconducting properties of SWNTs, the ability to vary carrier density or doping is a critical need for advances in nanoelectronics. Difficulties due to all surface atom makeup and the strong influence of the ambient surroundings have posed severe limitations until recently. Nitrogen impurity doping has been reported for multiwalled carbon nanotubes, but this process leads to highly defective geometries where simple tube structure is lost.[7] Strong acid purification induced oxygen containing groups (especially carboxyl groups) and subsequent chemical reactions to introduce covalent functional groups have also been examined as potential doping route but these approaches lead to partial loss of sidewall graphitic crystallinity and opened ends.[8] In addition, n-doping or electron injection is particularly more difficult since as-synthesized SWNTs usually exhibit p-type only behavior which has been attributed to

† Department of Materials Science and Engineering.
‡ Department of Physics.

(1) (a) Kam, N. W. S.; Liu, Z.; Dai, H. *J. Am. Chem. Soc.* **2005**, *127*, 12492. (b) Sazonova, V.; Yaish, Y.; Uestuenel, H.; Roundy, D.; Arias, T. A.; McEuen, P. L. *Nature (London)* **2004**, *431*, 284. (c) Schaller, R. D.; Klimov, V. I. *Phys. Rev. Lett.* **2004**, *92*, 186601. (d) Wang, C.; Shim, M.; Guyot-Sionnest, P. *Science* **2001**, *291*, 2390.
(2) (a) Erwin, S. C.; Zu, L.; Haftel, M. I.; Efros, A. L.; Kennedy, T. A.; Norris, D. J. *Nature* **2005**, *436*, 91. (b) Shim, M.; Guyot-Sionnest, P. *Nature* **2000**, *407*, 981.
(3) (a) Collins, P. G.; Bradley, K.; Ishigami, M.; Zettl, A. *Science* **2001**, *287*, 1801. (b) Sumanasekera, G. U.; Adu, C. K. W.; Fang, S.; Eklund, P. C. *Phys. Rev. Lett.* **2000**, *85*, 1096. (c) Heinze, S.; Tersoff, J.; Martel, R.; Derycke, V.; Appenzeller, J.; Avouris, Ph. *Phys. Rev. Lett.* **2002**, *89*, 6801. (d) Park, J.; McEuen, P. L. *Appl. Phys. Lett.* **2001**, *79*, 1363. (e) Shim, M.; Siddons, G. P. *Appl. Phys. Lett.* **2003**, *83*, 3564.
(4) (a) Zhou, X.; Park, J.-Y.; Huang, S.; Liu, J.; McEuen, P. L. *Phys. Rev. Lett.* **2005**, *95*, 146805. (b) Javey, A.; Guo, J.; Wang, Q.; Lundstrom, M.; Dai, H. *Nature* **2003**, *424*, 654.
(5) Yao, Z.; Kane, C. L.; Dekker: C. *Phys. Rev. Lett.* **2000**, *84*, 2941.
(6) Yu, M.-F.; Files, B. S.; Arepalli, S.; Ruoff, R. S. *Phys. Rev. Lett.* **2000**, *84*, 5552.
(7) Czerw, R.; Terrones, M.; Charlier, J.-C.; Blase, X.; Foley, B.; Kamalakaran, R.; Grobert, N.; Terrones, H.; Tekleab, D.; Ajayan, P. M.; Blau, W.; Ruehle, M.; Carroll, D. L. *NanoLett.* **2001**, *1*, 457.

10.1021/ja058551i CCC: $33.50

ambient oxygen adsorption both on the sidewalls as well as at the metal contacts.[3,9] Nonelectrical or electrochemical[10] n-doping processes to date include charge transfer doping from alkali metals,[11,12] thermal annealing in a vacuum (attributed to oxygen desorption),[13,14] choice of metal contacts,[15] and polymer adsorption.[16,17] For alkali metal doping and thermal annealing, vacuum atmosphere is required to achieve and to maintain n-type behavior. Alkali metal doping can also lead to undesirable irreversible structural changes. In multiwalled nanotubes, partial opening of the sidewalls has been observed upon alkali metal doping.[18] Lithium doping of SWNTs by applied electrochemical potential also leads to irreversible changes as observed by spectroscopic means.[19] Achieving n-channel conduction with choice of metal electrodes requires hydrogen annealing prior to metal deposition or poor performance limited by the large Schottky barrier is observed.[15] Adsorption of amine-rich polymers such as polyethylenimine (PEI) is a simple alternative approach which should in principle lead to noncovalent interaction that maintains structural integrity of SWNTs and therefore the high electronic performance.[16,17] Doping via polymer adsorption is very easy to achieve (e.g., spin-coating or simple exposure to polymer solutions), compatible with existing lithographic techniques for electrical contact deposition, and one of the very few methods that allows air-stable n-doping of SWNTs[16] with high performance.[17] While the simplicity of this doping method is very useful, how carriers in SWNTs are generated by simple adsorption of polymers has not been studied and needs to be elucidated. Compatibility of simple polymer adsorption with many measurement techniques (e.g., single nanotube Raman and electron transport measurements) may also facilitate understanding of charge-transfer processes in SWNTs.

With respect to metallic properties, studies of many novel phenomena occurring in 1-dimensional conductors may be hindered by extreme sensitivity to the local environment. One of the current topics of interest is the origin of the Breit−Wigner−Fano line shape of the tangential G-band in the Raman spectra of metallic nanotubes.[20] The Fano line shape arises from coupling to a continuum of states and has been thought to be intrinsic to metallic nanotubes.[21] Since the Fano line shape appears only in metallic tubes, the finite carrier density at the Fermi level is considered to be necessary to allow coupling to a continuum of states.[21] The line shape of metallic nanotubes' G-band and therefore the electron−phonon coupling has been shown to be highly sensitive to processing conditions, in particular, to oxidative purification conditions.[22] More recently, the Fano line shape being an intrinsic feature of metallic nanotubes has been questioned with evidences suggesting bundling effects inducing or enhancing the asymmetric line shape.[23,24] Our simple approach to changing the local chemical environment of isolated single nanotubes by polymer adsorption may provide insights into the intrinsic line shape which in turn should provide information on the nature of phonon−continuum coupling in these prototypical 1-dimensional conductors. Here, we examine how polymer adsorption affects the phonon modes of isolated individual SWNTs. Charge transfer doping in semiconducting SWNTs and changes in the G-band line shape (and therefore in the electron−phonon coupling) of metallic SWNTs upon simple adsorption of PEI are studied by micro-Raman measurements.

Experimental Section

Single-walled carbon nanotubes were synthesized on Si substrates with thermal oxide by established chemical vapor deposition methods.[25] Catalysts ($Fe(NO_3)_3 \cdot 9H_2O$ and Alumina in methanol) were deposited on deep-UV lithography patterned substrates. Growth of SWNTs was carried out in a tube furnace at 900 °C using ultrahigh purity CH_4 and H_2. For polymer adsorption, SWNTs grown on Si/SiO_2 substrates were immersed in 10 wt % PEI (Aldrich, $M_n = 10\,000$) in methanol overnight, washed with methanol, and dried with N_2 flow. Alternatively, 50 wt % PEI in methanol was spin-coated at 6000 rpm for 120 s directly on SWNTs on Si/SiO_2 substrates, allowed to stand for several hours, and rinsed with methanol followed by drying with N_2 flow. No significant differences were observed in the two methods. As-synthesized SWNTs were allowed to equilibrate in air for several days prior to measurements. Atomic force microscope (AFM) images were collected on a Digital Instruments Dimension 3100. Raman measurements were carried out on a Jobin Yvon LabRam HR 800 micro-Raman spectrometer with 633 nm (1.96 eV) and 785 nm (1.58 eV) excitation sources under air ambient conditions. The maximum intensity used was ~3 mW (~3 μW) for 633 nm (785 nm) laser with spot size of ~1 μm in diameter for 100× air objective. Even at the maximum intensity for 633 nm excitation, we do not observe any changes in the Raman spectra due to extended laser exposure. Lower intensity measurements with 633 nm as well as the 3 orders of magnitude smaller intensity of 785 nm excitation show same results. Thermoelectrically cooled CCD has a resolution of ~0.3 cm^{-1} per pixel which is approximately the spectral resolution of the instrument. All Raman spectra shown are the raw data collected.

(8) (a) Liu, J.; Rinzler, A. G.; Dai, H. J.; Hafner, J. H.; Bradley, R. K.; Boul, P. J.; Lu, A.; Iverson, T.; Shelimov, K.; Huffman, C. B.; Rodriguez-Macias, F.; Shon, Y. S.; Lee, T. R.; Colbert, D. T.; Smalley, R. E. *Science* **1998**, *280*, 1253. (b) Chen, J.; Hamon, M. A.; Hu, H.; Chen, Y. S.; Rao, A. M.; Eklund, P. C.; Haddon, R. C. *Science* **1998**, *282*, 95. (c) Dettlaff-Weglikowska, U.; Benoit, J. M.; Chiu, P. W.; Graupner, R.; Lebedkin, S.; Roth, S. *Curr. Appl. Phys.* **2002**, *2*, 497.

(9) Dukovic, G.; White, B. E.; Zhou, Z.; Wang, F.; Jockusch, S.; Steigerwald, M. L.; Heinz, T. F.; Friesner, Ri. A.; Turro, N. J.; Brus, L. E. *J. Am. Chem. Soc.* **2004**, *126*, 15269.

(10) (a) Kazaoui, S.; Minami, N.; Matsuda, N.; Kataura, H.; Achiba, Y. *Appl. Phys. Lett.* **2001**, *78*, 3433. (b) Kavan, L.; Rapta, P.; Dunsch, L.; Bronikowski, M. J.; Willis, P.; Smalley, R. E. *J. Phys. Chem. B* **2001**, *105*, 10764. (c) Kavan, L.; Dunsch, L. *Nano Lett.* **2003**, *3*, 969.

(11) (a) Rao, A. M.; Eklund, P. C.; Bandow, S.; Thess, A.; Smalley, R. E. *Nature (London)* **1997**, *388*, 257. (b) Bockrath, M.; Hone, J.; Zettl, A.; McEuen, P. L.; Rinzler, A. G.; Smalley, R. E. *Phys. Rev. B* **2000**, *61*, R10606.

(12) (a) Chen, G.; Furtado, C. A.; Kim, U. J.; Eklund, P. C. *Phys. Rev. B* **2005**, *72*, 155406. (b) Chen, G.; Furtado, C. A.; Bandow, S.; Iilima, S.; Eklund, P. C. *Phys. Rev. B* **2005**, *71*, 045408.

(13) Shim, M.; Back, J. H.; Ozel, T.; Kwon, K.-W. *Phys. Rev. B* **2005**, *71*, 205411.

(14) Derycke, V.; Martel, R.; Appenzeller, J.; Avouris, Ph. *NanoLett.* **2001**, *1*, 453.

(15) (a) Radosavljevic, M.; Freitag, M.; Thadani, K. V.; Johnson, A. T.; *Nano Lett.* **2002**, *2*, 761. (b) Nosho, Y.; Ohno, Y.; Kishimoto, S.; Mizutani, T. *Appl. Phys. Lett.* **2005**, *86*, 073105.

(16) Shim, M.; Javey, A.; Kam, N. W. S.; Dai, H. *J. Am. Chem. Soc.* **2001**, *123*, 11512.

(17) (a) Siddons, G. P.; Merchin, D.; Back, J. H.; Jeong, J. K.; Shim, M. *NanoLett.* **2004**, *4*, 927. (b) Ozel, T.; Gaur, A.; Rogers, J. A.; Shim, M. *NanoLett.* **2005**, *5*, 905.

(18) Zhou, O.; Fleming, R. M.; Murphy, D. W.; Chen, C. H.; Haddon, R. C.; Ramirez, A. P.; Glarum, S. H. *Science* **1994**, *263*, 1744.

(19) Claye, A.; Rahman, S.; Fischer, J. E.; Sirenko, A.; Sumanasekera, G. U.; Eklund, P. C. *Chem. Phys. Lett.* **2001**, *333*, 16.

(20) (a) Kataura, H.; Kumazawa, Y.; Maniwa, Y.; Umezu, I.; Suzuki, S.; Ohtsuka, Y.; Achiba, Y. *Synth. Met.* **1999**, *103*, 2555. (b) Alvarez, L.; Righi, A.; Guillard, T.; Rols, S.; Anglaret, E.; Laplaze, D.; Sauvajol, J.-L. *Chem. Phys. Lett.* **2000**, *316*, 186.

(21) Brown, S. D. M.; Jorio, A.; Corio, P.; Dresselhaus, M. S.; Saito, R.; Kneipp, K. *Phys. Rev. B* **2001**, *63*, 155414.

(22) Yu, Z.; Brus, L. E. *J. Phys. Chem. A* **2000**, *104*, 10995.

(23) Jiang, C.; Kempa, K.; Zhao, J.; Schlecht, U.; Kolb, U.; Basche, T.; Burghard, M.; Mews, A. *Phys. Rev. B* **2002**, *66*, 161404.

(24) Paillet, M.; Poncharal, Ph.; Zahab, A.; Sauvajol, J.-L.; Meyer, J. C.; Roth, S. *Phys. Rev. Lett.* **2005**, *94*, 237401.

(25) Kong, J.; Soh, H. T.; Cassell, A. M.; Quate, C. F.; Dai, H. *Nature (London)* **1998**, *395*, 878.

Results and Discussion

From chiral index assignment[26,27] to examining electronically selective chemical reactivity,[28] Raman spectroscopy has been a powerful characterization tool for SWNTs. Here, we exploit the ability to carry out resonant Raman measurements at the single nanotube level[26,29] to examine charge transfer doping and the Fano line shape evolution in SWNTs upon polymer adsorption. We first describe our approach to examining isolated individual SWNTs before and after PEI adsorption by micro-Raman measurements. Diameter dependent spectral response to charge transfer from PEI to semiconducting SWNTs are then examined followed by a discussion on the strikingly different behavior of metallic tubes.

Raman Measurements on Isolated Single Nanotubes. While Raman spectroscopy has been extensively used to characterize charge-transfer processes in SWNTs,[11,12,30] most studies have been limited to ensemble measurements. To examine charge transfer at the single nanotube level, it is critical to ensure that only one SWNT contributes to the observed signal[31] and that the same nanotube can be located before and after the charge-transfer step. A combination of micro-Raman measurements, facile method of doping via polymer adsorption, and low density of SWNTs allows us to examine spectroscopic changes at the single nanotube level. Figure 1 compares a Raman map obtained from the integrated intensity of the tangential G-band of an area near a patterned catalyst with the same area AFM image. The bright region at the top of Figure 1A is the patterned catalyst where there is a very high density of SWNTs. The AFM image in Figure 1B shows the same area. Note that there is a larger number of SWNTs in the AFM image due to the limited number of SWNTs being resonant with the laser excitation source. However, where there are appreciable intensities of the G-band region, a nanotube can be seen in the AFM image. Corresponding nanotubes in the Raman map and the AFM image are labeled 1−4. As Figure 1B shows, there is a significantly large density of SWNTs within about 1 μm from the catalyst pattern. To ensure that only one SWNT contributes to the Raman signal, only spots that are ~2 μm or further away from the patterned catalysts where the typical density of SWNTs is much less than 1 μm^{-2} (as shown by the AFM image) are used for analysis.

To ensure that the same nanotube is examined before and after PEI adsorption, the patterned catalysts as well as lithographically etched markers are used for alignment. Once the resonant SWNT of interest is located from the Raman signal (usually by the G-band), a smaller area is scanned to ensure collection at the same spot (within the laser spot size limited spatial resolution). Samples are also mounted on a rotational stage to ensure same angular alignment (within ~0.1°) with respect to the laser polarization. Figure 2 shows the radial breathing mode (RBM) and G-band maps of the same area before (A and B) and after (E and F) PEI adsorption. Notice that the intensity of the Raman active modes can vary along the length of the nanotube. While normalizing intensities with respect to the substrate Si phonon mode has been carried out to compare relative intensities,[26] we examine only the line widths and frequency shifts upon PEI doping due to this variation in intensity and laser spot size limited spatial resolution of ~1 μm. For most resonant SWNTs, no significant differences in the line widths and frequencies of the RBM and the G-band have been found along the length of the SWNT as shown in Figure 2 prior to PEI adsorption. Changes in the RBM and/or the G-band frequencies that we have observed occasionally are usually associated with abrupt changes in the direction of the nanotube. This may be due to defects causing a "kink" and a change in chirality along a same SWNT or simply the beginning of another SWNT which happens to have a partial spatial overlap.

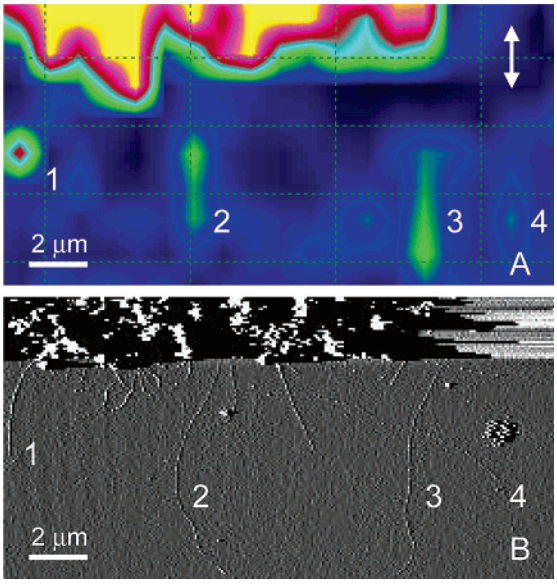

Figure 1. (A) Raman map of integrated intensity around the G-band (1575−1610 cm^{-1}). The map is collected using 633 nm (1.96 eV) excitation source at 1 μm scan step. The laser polarization is indicated by the double-headed arrow at the top-right corner. The bright area at the top of the figure is the patterned catalysts which can serve to facilitate alignment and locating SWNTs. The small spot left of SWNT labeled 3 in the Raman map is due to higher background noise. (B) Atomic force microscope image of the same area. Numbers 1−4 indicate the corresponding SWNTs in Raman map and AFM image.

The spectra shown in Figure 2 are collected at the positions indicated by the arrows in the Raman maps. These are the actual spectra collected during the mapping measurements. The appearance of the RBM peak at 142.4 cm^{-1} and the resonance with 633 nm (1.96 eV) laser excitation source indicate that this is a semiconducting SWNT with a possible chiral index (n,m) of (19,5). For the low-frequency RBM region, the spectra are fitted with a linear background and a single Lorentzian. The numbers next to the RBM peaks are the peak position in cm^{-1} and the full width at half-maximum (fwhm) in parentheses from the least-squares fit. There are no changes in the spectral position and the line width of the RBM along the length of the SWNT or upon PEI adsorption for this SWNT. The difference in the

(26) Jorio, A.,; Saito, R.; Hafner, J. H.; Lieber, C. M.; McClure, T.; Dresselhaus, G.; Dresselhaus, M. S. *Phys. Rev. Lett.* **2001**, *86*, 1118.
(27) Rao, A. M.; Chen, J.; Richter, E.; Schlecht, U.; Eklund, P. C.; Haddon, R. C.; Venkateswaran, U. D.; Kwon, Y.-K.; Tomanek, D. *Phys. Rev. Lett.* **2001**, *86*, 3895.
(28) Wang, C.; Cao, Q.; Ozel, T.; Gaur, A.; Rogers, J. A.; Shim, M. *J. Am. Chem. Soc.* **2005**, *127*, 11460.
(29) Hartschuh, A.; Pedrosa, H. N.; Novotny, L.; Krauss, T. D. *Science* **2003**, *301*, 1354.
(30) (a) Cronin, S. B.; Barnett, R.; Tinkham, M.; Chou, S. G.; Rabin, O.; Dresselhaus, M. S.; Swan, A. K.; Unlu, M. S.; Goldberg, B. B. *Appl. Phys. Lett.* **2004**, *84*, 2052. (b) Murakoshi, K.; Okazaki, K. *Electrochim. Acta* **2005**, *50*, 3069.
(31) Jorio, A.; Souza, F.; Dresselhaus, G.; Dresselhaus, M. S.; Swan, A. K.; Unlu, M. S.; Goldberg, B. B.; Pimenta, M. A.; Hafner, J. H.; Lieber, C. M.; Saito, R. *Phys. Rev. B* **2002**, *65*, 155412.

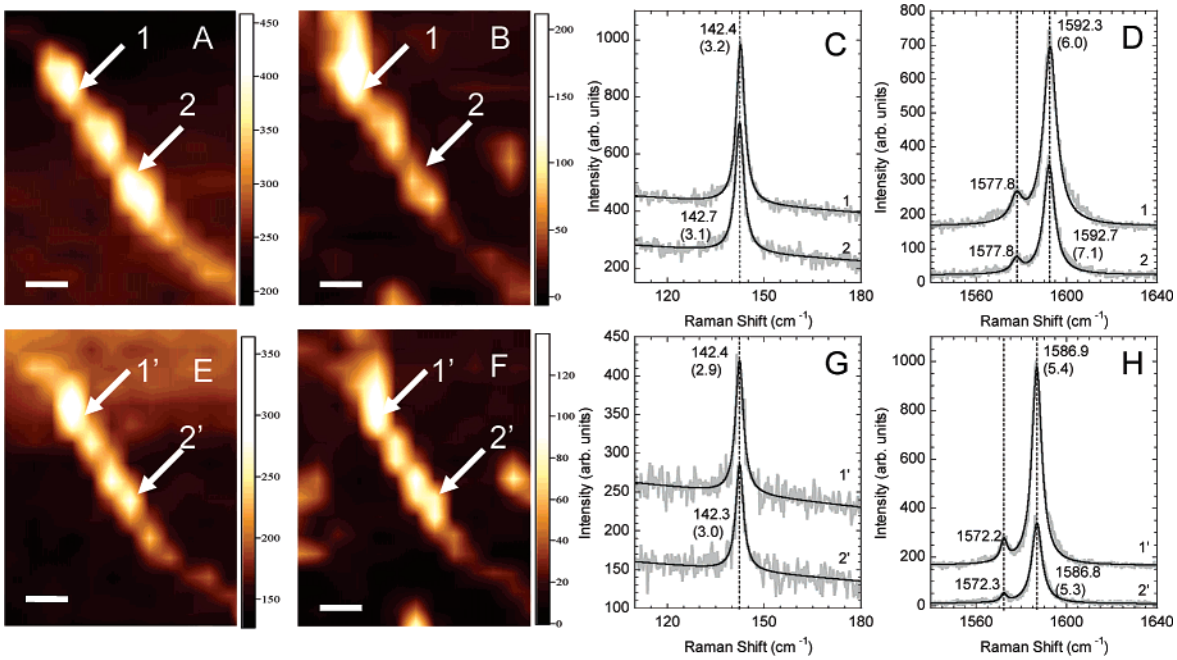

Figure 2. Raman maps of the radial breathing mode (A and E) and the G-band (B and F) regions of the same semiconducting single-walled carbon nanotube before (A and B) and after (E and F) n-doping with polyethylenimine. All scale bars are 1 μm. Spectra at the spots indicated by the arrows in the Raman map are shown in (C) and (D) for as-synthesized and (G) and (H) for after polymer adsorption. Grey lines are the data and the black lines are the Lorentzian curve fits. Raman maps are collected with 633 nm (1.96 eV) laser excitation. Spectra are offset for clarity.

frequency for spectra labeled 1 and 2 (which are taken at the spots labeled correspondingly in the RBM map) is less than 0.3 cm^{-1} which is smaller than our resolution limit. The difference before and after PEI adsorption is also less than our resolution. The fwhm of the Lorentzian of the RBM peak in all four spectra in Figure 2C,G are within 0.3 cm^{-1} of 3 cm^{-1}. The narrow line widths of both RBM and the G band peaks approach that of the reported natural line widths[32] of ~3 cm^{-1} for RBM and ~5 cm^{-1} for the most intense G-band peak further confirming that individual isolated SWNTs are being measured. We note that a few semiconducting SWNTs (mostly relatively small diameter tubes) exhibit small but nonnegligible RBM frequency shift upon PEI adsorption (up to ~2 cm^{-1} shift has been observed). In halogen and alkali metal doping of nanotube bundles, spectral shifts of the RBMs may be expected due to intercalation between SWNTs and large shifts and disappearance of RBMs have been observed.[11a,33] In the absence of such intercalation effects, as is the case in our isolated individual SWNTs, RBM frequency may be constant since charge injection is expected to change the in-plane C−C bond lengths but not necessarily the out-of-plane vibrational modes. The few RBM spectral shifts that we observe may be associated with changes in the surrounding as observed in comparison between on-substrate and suspended SWNTs[34] rather than with electron injection.

Diameter-Dependent Doping of Semiconducting Nanotubes. One of the key features that has been used to examine charge-transfer processes in carbon nanotubes as well as in graphite intercalation compounds is the spectral changes in the tangential G-band of the Raman spectra.[12,19,35] The G-bands in Figure 2D and 2H are fitted to two Lorentzians. Much like the RBM, there are no significant frequency variations along the length of the SWNT. However, unlike the RBM, there is a large shift in the spectral position of the G-band upon PEI adsorption. The most intense peak at higher frequency (G^+) downshifts from 1592.3 to 1586.9 cm^{-1} and the lower frequency peak (G^-) also exhibits very similar downshift of 5.5 cm^{-1} upon PEI doping. The same changes are seen along the full length of the SWNT upon PEI adsorption. This downshift in the G-band is consistent with C−C bond length expansion expected upon electron injection and as observed in alkali metal doping of nanotube and graphite systems.[12,35] The downshift of ~6 cm^{-1} is comparable to the ~8 cm^{-1} shift observed in electrochemical doping with K and Li.[19] As a simple guide, if we assume the same G-band shift ($\Delta\omega_G$) to doping fraction change (ΔQ) ratio $\alpha \equiv \Delta\omega_G/\Delta Q \sim 370$ cm^{-1}/electrons per C atom as reported for alkali metal electrochemical doping,[19] this downshift corresponds to $\Delta Q \approx 0.02$. Considering that the amine groups of PEI are separated by 2 C atoms with a mixture of primary, secondary, and tertiary amines (i.e., possible differences in electron donating ability) and that the branched structure of the polymer is unlikely to yield close-packed chains, this magnitude of doping fraction change may be expected. However, as shown below, there is a strong diameter dependence on the G-band shift upon PEI doping.

Figure 3 shows the Raman spectra of two different diameter semiconducting SWNT before and after PEI adsorption. Assuming d(nm) = 248/ω_{RBM}(cm^{-1}),[26] Figure 3A−C correspond to a 1.7 nm diameter SWNT and Figure 3D−F to a 0.85 nm diameter SWNT. With the laser excitation at 633 nm (1.96 eV),

(32) (a) Jorio, A.; Fantini, C.; Dantas, M. S. S.; Pimenta, M. A.; Souza, A. G.; Samsonidze, Ge. G.; Brar, V. W.; Dresselhaus, G.; Dresselhaus, M. S.; Swan, A. K.; Unlu, M. S.; Goldberg, B. B.; Saito, R. *Phys. Rev. B* **2002**, *66*, 115411. (b) Iliev, M. N.; Litvinchuk, A. P.; Arepalli, S.; Nikolaev, P.; Scott, C. D. *Chem. Phys. Lett.* **2000**, *316*, 217.
(33) Bendiab, N.; Righi, A.; Anglaret, E.; Sauvajol, J. L.; Duclaux, L.; Beguin, F. *Chem. Phys. Lett.* **2001**, *339*, 305.
(34) Zhang, Y.; Zhang, J.; Son, H.; Kong, J.; Liu, Z. *J. Am. Chem. Soc.* **2005**, *127*, 17156.
(35) (a) Eklund, P. C.; Dresselhaus, G.; Dresselhaus, M. S.; Fischer, J. E. *Phys. Rev. B* **1977**, *16*, 3330. (b) Dresselhaus, M. S.; Dresselhaus, G. *Adv. Phys.* **1981**, *30*, 139.

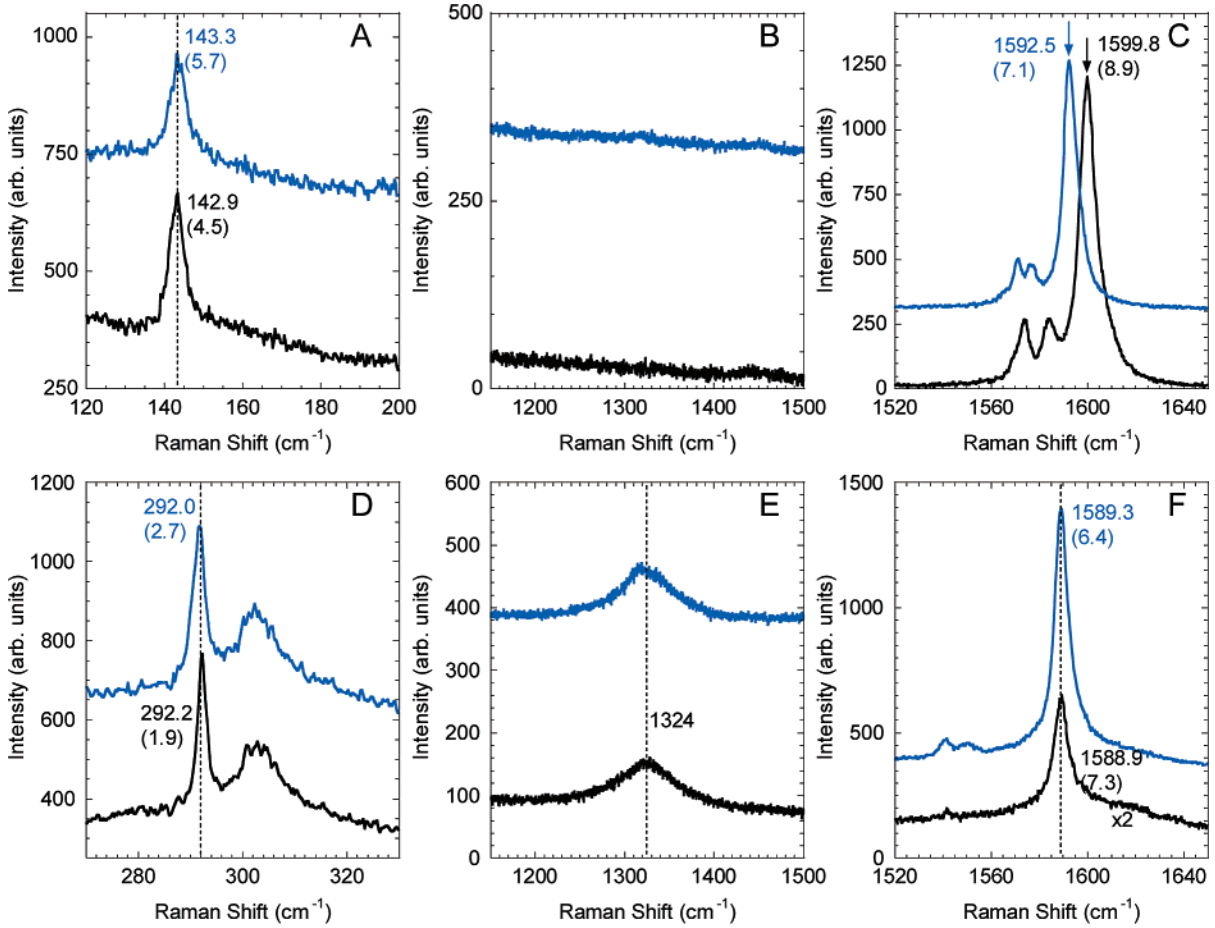

Figure 3. Raman spectra of 1.7 nm (A−C) and 0.85 nm (D−F) diameter single-walled carbon nanotubes before and after polymer doping. Radial breathing mode (A and D), disorder mode (B and E), and the G-band regions are shown. In all cases, lower black curves are as-synthesized nanotube spectra and the upper blue curves are after polyethylenimine adsorption. The numbers next the peaks indicate the spectral position in cm-1 and the numbers in the parentheses are fwhm from Lorentzian curve fits. Broader feature at ~303 cm-1 in (D) is from the Si substrate. All spectra are obtained with 633 nm (1.96 eV) laser excitation. Spectra are offset for clarity.

the RBM frequencies correspond to possible chiral indices of (15,10) for the larger and (8,4) for the smaller tube.[26a] The absence of the disorder (D) mode at ~1300 cm^{-1} for the larger diameter SWNT indicates that this tube is free of amorphous carbon residues. Isolated semiconducting SWNTs that we have examined usually exhibit very small or no D-mode. When it is observed, the D-band is often associated with relatively small diameter SWNTs as shown in Figure 3E or metallic SWNTs. Unlike covalent chemical reactions,[28] PEI adsorption usually leads to no significant changes in the D-mode for semiconducting SWNTs. In the small diameter semiconducting SWNT shown in Figure 3D−F, there is an actual reduction in the relative intensity of D-band with respect to the G-band. In all semiconducting tubes that we have examined, no increase in the D-band is observed confirming the expectation that PEI adsorption on semiconducting SWNTs is noncovalent.

The G^+ (G^-) peak for the larger diameter SWNT shown in Figure 3C exhibits a similar downshift of 7.3 (7.1) cm^{-1} upon PEI doping as the semiconducting SWNT of similar diameter shown in Figure 2. Surprisingly, there is no significant change in the spectral position of the G-band for the small diameter SWNT in Figure 3F. The diameter (d) dependence of the change in the G-band of semiconducting SWNTs upon PEI adsorption is shown in Figure 4. The tentative chiral index (n, m) assignment for these SWNTs is given in the Supporting Information. There is a strong diameter dependence of the magnitude of the downshift for both G^+ and G^- peaks. Larger diameter SWNTs show significantly larger downshift upon PEI doping whereas smaller diameter tubes show little or no change. Two SWNTs with $d \approx 0.9$ nm show small upward shifts in the G^+ peak which may be an analogous effect to the anomalous C−C bond contraction observed at low doping fractions of alkali

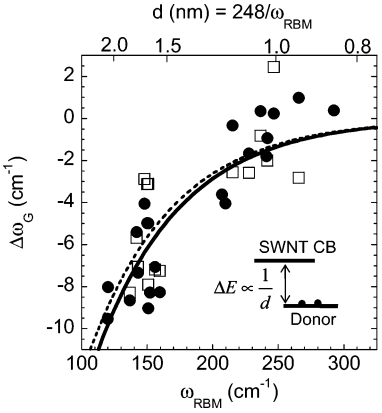

Figure 4. (A) Diameter dependence of the spectral shift of the G-band peaks, G^+ (filled circles) and G^- (open squares), upon n-doping with polyethylenimine. The curves are least-squares fits for carrier thermal ionization process as described in the text. Solid (dashed) line corresponds to fit to G^+ (G^-) peak shift. Inset is a schematic energy level diagram.

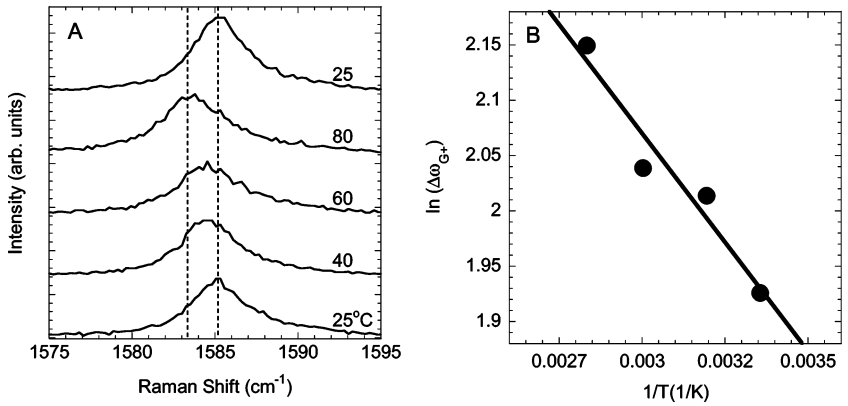

Figure 5. (A) G-band region of spectra of a 1.75 nm diameter SWNT doped with polyethylenimine at the indicated temperatures. The top spectrum is collected after cooling back down to room temperature. (B) Temperature dependence of the G+ peak shift. The solid line is a least-squares fit as discussed in the text.

metal doping,[12] but further studies are needed to elucidate this effect.

However, the overall trend in the diameter dependence of the G-band spectral shift shown in Figure 4 may be explained by a diameter dependent activation barrier for thermal ionization of electrons from the donor PEI to the semiconducting SWNTs. For simplicity, we assume that n is directly equal to the number of electrons ionized from PEI per unit length. With the donor energy level at ΔE below the conduction band edge, the linear density of carriers is then approximated by

$$n = N_{\mathrm{D}} \exp\left(-\frac{\Delta E}{kT}\right) \tag{1}$$

where N_{D} is the linear density of donors and kT is the thermal energy. A schematic energy diagram is shown in the inset of Figure 4. Following the results from alkali metal electrochemical doping of SWNTs,[19] we assume that the G-band spectral shift due to electron injection is linearly proportional to the doping fraction change (i.e., $\alpha \equiv \Delta\omega_{\mathrm{G}}/\Delta Q =$ constant). Assuming no carriers prior to PEI adsorption, the doping fraction change is $\Delta Q = n/N_{\mathrm{C}}$ where N_{C} is the linear density of C atoms of the SWNT. Then the G-band spectral shift upon PEI adsorption is given by

$$\Delta\omega_{\mathrm{G}} = \alpha\frac{N_{\mathrm{D}}}{N_{\mathrm{C}}} \exp\left(-\frac{\Delta E}{kT}\right) \tag{2}$$

The solid (dashed) curve in Figure 4 is the least-squares fit to eq 2 for G^+ (G^-) peak shift. Here, the preexponential $\alpha N_{\mathrm{D}}/N_{\mathrm{C}}$ is assumed to be independent of diameter and ΔE to be linearly proportional to the band gap or inversely to diameter d. The fit gives $\alpha N_{\mathrm{D}}/N_{\mathrm{C}} \approx 60$ cm^{-1} and $\Delta E \approx 0.1$ eV·nm/d.

To further verify the thermal ionization process for electron injection into the conduction band, we also show temperature dependence of G-band shift for a PEI doped SWNT in Figure 5. G-band region of the Raman spectra of a SWNT exhibiting RBM at 142 cm^{-1} is shown in Figure 5A at the indicated temperatures. In Figure 5B, the log of the shift in the G^+ peak with respect to the original G^+ peak frequency prior to PEI adsorption is plotted as a function of inverse temperature. Linear fit to the equation, $\ln(\Delta\omega_{\mathrm{G}}) = \ln(\alpha N_{\mathrm{D}}/N_{\mathrm{C}}) - \Delta E/kT$, gives $\alpha N_{\mathrm{D}}/N_{\mathrm{C}} \approx 30$ cm^{-1} and $\Delta E \approx 34$ meV for this 1.75 nm diameter tube. If we use $\alpha = 370$ cm^{-1} (ref 19) then the ratio of donors

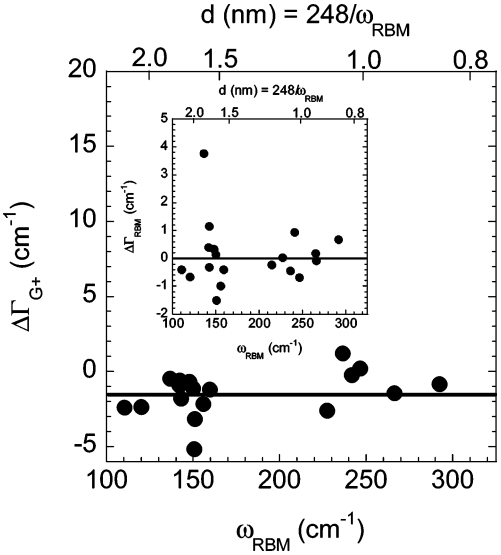

Figure 6. Line width (full width at half-maximum) change of radial breathing mode ($\Delta\Gamma_{\mathrm{RBM}}$) and the main feature in the G band ($\Delta\Gamma_{\mathrm{G+}}$) for different diameter SWNTs upon doping with PEI. On average, the radial breathing mode (inset) shows no change and the G-band shows very slight line narrowing.

to C atoms in the SWNT $N_{\mathrm{D}}/N_{\mathrm{C}} \approx 1/12$, which is reasonable considering the density of N atoms on PEI. Remarkably, the values obtained here for $\alpha N_{\mathrm{D}}/N_{\mathrm{C}}$ and ΔE are very close to the values independently obtained from the diameter dependence shown in Figure 4 ($\alpha N_{\mathrm{D}}/N_{\mathrm{C}} = 30$ cm^{-1} from Figure 5 and 60 cm^{-1} from Figure 4, and $\Delta E = 34$ meV from Figure 5 and 57 meV from Figure 4). The small differences may be due to our simplification such as $\Delta\omega_{\mathrm{G}}$ being linearly proportional to the number of charges injected and independent of SWNT diameter. While our treatment of the carrier injection process is admittedly a simple one (e.g., assumption of linear $\Delta\omega_{\mathrm{G}}$ to ΔQ relation and neglecting potential p-doping effects of ambient oxygen, etc.), it is consistent with and gives an intuitive understanding of the diameter dependence observed here with reasonable values of the activation energies for thermal ionization of carriers.

While the spectral shift in the G-band exhibits a strong diameter effect, the line width change is independent of diameter. The inset of Figure 6 shows the changes in the line widths of the RBM ($\Delta\Gamma_{\mathrm{RBM}}$) of semiconducting SWNTs upon PEI

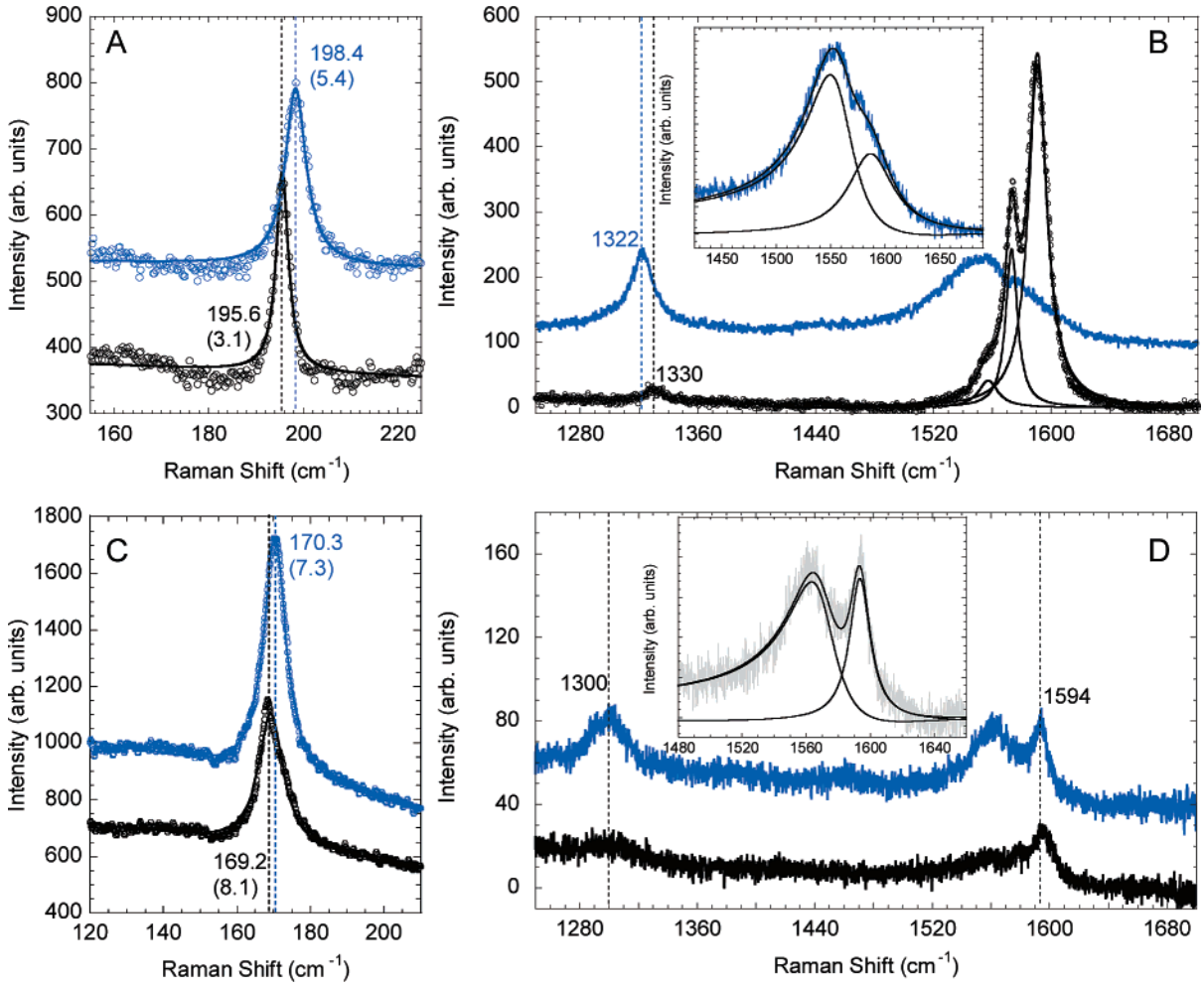

Figure 7. Spectral response of a 1.3 nm (A and B) and a 1.5 nm (C and D) diameter metallic nanotubes upon polyethylenimine adsorption. In all spectra, lower black curves and symbols are before polymer adsorption and the upper blue curves and symbols are after. The after polymer adsorption spectra are offset for clarity. The spectra in A and B are collected with 633 nm (1.96 eV) excitation and the spectra in C and D are collected with 785 nm (1.58 eV) excitation source. The G-band region around 1590 cm^{-1} in B for the spectrum prior to polymer adsorption is fitted to 3 Lorentzians. In B and D, the insets are the G-band regions after polyethylenimine adsorption with Fano and Lorentzian curve fitting shown in black solid lines.

adsorption. There is no significant broadening suggesting that PEI adsorption does not cause changes in the extrinsic (e.g., additional scattering sites due to polymer-nanotube interaction, mechanical deformation, etc.) and intrinsic (e.g., perturbation to the electronic wave functions, Raman resonance conditions, etc.) properties that contribute to the observed line widths of semiconducting SWNTs. These results are consistent with our previous electrical measurements where PEI adsorption has led to electron mobilities similar to as-fabricated device hole mobilities suggesting that PEI does not induce additional scattering.[17] The change in the line width of the G^+ peak ($\Delta\Gamma_{G+}$) is shown in Figure 6. Unlike ensemble measurements on doping processes, there is, if any, a slight line narrowing of $1-3$ cm^{-1} for most isolated semiconducting tubes. In alkali metal doping, $\sim$50 cm^{-1} broadening of the fwhm of the G-band has been observed at the onset of the downshift for the ensemble of nanotubes.[12] During this G-band downshifting stage of doping, the Lorentzian line shape continuously changes to an asymmetric Fano line shape.[12] However, our results for isolated single nanotubes shown in Figure 6 are from Lorentzian curve fits without significant line broadening (see also Figures 2H and 3C) suggesting that semiconducting SWNTs are not likely to contribute to the appearance of the asymmetric line shape, at least at the relatively low levels of doping that we can achieve with PEI. On the basis of the diameter dependence of the G-band spectral shift in Figure 4, semiconducting SWNTs will contribute to inhomogeneous line broadening rather than line shape symmetry change in the ensemble. In contrast, metallic SWNTs exhibit distinctly different behavior which may have a more profound effect on the overall line shape evolution observed in the ensemble. More importantly, the different spectral response may have implications on the intrinsic line shape of metallic SWNT G-band which in turn will have consequences on the interpretation of electron−phonon coupling from Raman measurements as discussed below.

Metallic Nanotubes and Intrinsic Phonon Line Shape. Figure 7 shows the Raman spectra of two different metallic SWNTs before and after PEI adsorption. There is a slight shift in the RBM (A and C) in both tubes. However, this shift varies from nanotube to nanotube with average shift of less than $+1$ cm^{-1} for the 10 metallic tubes we have examined. There are two strikingly different spectral responses compared to the semiconducting tubes. For the two metallic nanotubes shown in Figure 7, a large enhancement of the D mode at $\sim$1300 cm^{-1} and a broadening of the G-band are observed. The ratio of integrated intensities of D-band to G-band increases by about a

factor of 2 on average for 10 metallic tubes examined. This enhancement of D-band upon PEI adsorption only in metallic SWNTs is consistent with the claim in ref 36 that amine functional groups have higher affinity toward metallic tubes (which in turn has been used to explain the effective separation of metallic tubes from semiconducting ones). For the metallic nanotubes that exhibit broad G-band prior to PEI adsorption, the asymmetric Fano line shape is maintained. On the other hand, when we observe relatively narrow line shapes that can be fitted to two to four Lorentzians, significant broadening as shown in Figure 7 is observed. These changes are not likely to arise from photochemical reactions of PEI since (1) the laser excitation sources are in the visible/near-IR range where PEI does not absorb and (2) no noticeable differences are observed when these measurements are carried out at very low intensities. In fact, spectra shown in Figure 7C,D are collected with 785 nm (1.58 eV) laser excitation at $\sim 3\ \mu$W.

The origin of the broad, asymmetric feature in the G band of metallic SWNTs is currently under intense investigation.[20−23] Initially, this G-band feature has been attributed to phonon−plasmon coupling in the presence of conduction electrons with increasing curvature (due to decreasing diameter) leading to stronger coupling.[21] More recently, two reports have suggested that the asymmetric Fano line shape arises from effects induced by bundling of multiple tubes which enhances phonon-plasmon coupling.[23,24] Two reports suggest that the intrinsic line shape is not the asymmetric Fano line shape. [24,37] Shown in the main panel of Figure 7B for the spectrum prior to PEI adsorption is a three Lorentzian fit for the G-band. The fitting leads to narrow lines at 1557, 1573, and 1591 cm^{-1} with corresponding fwhms of 16, 10, and 15 cm^{-1} which are comparable to the line widths observed in isolated semiconducting tubes. The broadened asymmetric line shape after PEI adsorption, on the other hand, requires a Fano line given by

$$I(\omega) = I_o \frac{[1 + (\omega - \omega_o)/q\Gamma]^2}{1 + [(\omega - \omega_o)/\Gamma]^2} \qquad (3)$$

and a Lorentzian for fitting. Here, ω_o is the Fano line spectral position with intensity I_o, $1/q$ is the measure of phonon coupling to a continuum of states, and Γ is the line width. From the fit shown in Figure 7B inset, the coupling parameter $1/q = -0.28$, which is slightly larger than previously reported values.[21,22] Spectral response of another metallic SWNT upon PEI adsorption is shown in Figure 7C,D. Similar values of the coupling parameter ($1/q = -0.3$) as that of the tube in Figure 7B is obtained from the fit shown in the inset of 7D. The important point is that, in addition to the enhancement of D-mode, the initial relatively weak or negligible Fano line shape for the lower frequency G-band feature (G^-) becomes significantly enhanced upon PEI adsorption in both cases whereas the higher frequency mode (G^+) remains Lorentzian in line shape similar to the line shapes observed in ref 21.

Currently proposed mechanisms for the appearance of Fano line shape in the Raman spectra of metallic SWNTs involve coupling of discrete phonons to acoustic/quasiacoustic or a potentially low-lying optical plasmons.[21,38,39] For the acoustic/quasiacoutic plasmon cases, "defects" are invoked to allow phonon−plasmon coupling. On the basis of the average diameter dependence, Brown et al. have suggested that the nanotube curvature facilitates Fano coupling of the lower frequency G^- mode (where the atomic displacements are along the circumference of the tube) to the plasmon continuum but not the higher frequency G^+ mode which has atomic displacements along the tube axis.[21] On the other hand, Jiang et al.[23] and Paillet et al.[24] have experimentally shown that bundling is an important factor in the appearance/enhancement of the asymmetric G-band line shape consistent with Kempa's theoretical treatment[38] of gapless quasiacoustic plasmons where excitations of plasmon−phonon hybrid modes introduce the Fano line shape in the Raman spectra and bundling leads to a strong enhancement of the asymmetric line shape. In addition, Bose et al.[38] have proposed phonon coupling to a low-lying optical plasmon that can explain both higher frequency Lorentzian and lower frequency Fano line shapes in metallic tube G-band features without invoking curvature or bundling effects. Our observation of initial all-Lorentzian line shapes of metallic tubes converting to Fano + Lorentzian line shape after PEI adsorption along with a concurrent enhancement of D-band suggests that the Fano coupling to a plasmon continuum may be mediated by in-plane disorder. Intrinsic line shape of isolated individual metallic nanotubes may be Lorentzian and this in-plane disorder induced by changes in the local chemical environment (in our case, the adsorption of PEI) can turn on or strongly enhance Fano coupling.

We finally note that Yu and Brus have previously reported enhanced Fano line shape in nanotube bundles upon laser heating and thermally induced degassing of oxidizing molecules adsorbed from strong acid processing conditions.[22] While our samples are prepared by CVD method where the growth is the very last step and therefore no intentional oxidation process is introduced, there are many reports of oxygen adsorption induced changes in the electronic properties of SWNTs.[3,9,13] Then the variations in the initial line shape (i.e., some with all Lorentzian and some with a combination of Lorentzian and Fano shapes) of the G-band of as-synthesized isolated metallic tubes that we observe and also reported by Jorio et al.[31] may be attributed to the different degree of ambient air atmosphere induced changes (e.g., different degrees of oxidation). These observations indicate that molecular adsorption on metallic SWNTs can have dramatic effects on the G-band line shape and therefore on the electron−phonon coupling. At the very least, these results emphasize the importance of the local chemical environment/molecular adsorption on phonon scattering in carbon nanotubes. Further studies are needed and are underway to address contributions of the local chemical environment (in particular the chemical nature/atomic details of the induced disorder) and the tube curvature to the intrinsic line shape of metallic tubes.

Conclusions

We have presented Raman studies on doping of SWNTs by PEI adsorption at the single nanotube level. Distinctly different spectral responses from semiconducting and metallic SWNTs

(36) Maeda, Y.; Kimura, S.-i.; Kanda, M.; Hirashima, Y.; Hasegawa, T.; Wakahara, T.; Lian, Y.; Nakahodo, T.; Tsuchiya, T.; Akasaka, T.; Lu, J.; Zhang, X.; Gao, Y.; Yu, Y.; Nagase, S.; Kazaoui, S.; Minami, N.; Shimizu, T.; Tokumoto, H.; Saito, R. *J. Am. Chem. Soc.* **2005**, *127*, 10287.
(37) Oron-Carl, M.; Hennrich, F.; Kappes, M. M.; Lohneysen, H. v.; Krupke, R. *NanoLett.* **2005**, *5*, 1761.
(38) Kempa, K. *Phys. Rev. B* **2002**, *66*, 195406.
(39) Bose, S. M.; Gayen, S.; Behera, S. N. *Phys. Rev. B* **2005**, *72*, 153402.

are observed. Strong diameter dependence of the G-band spectral shift of semiconducting SWNTs has been found which may be attributed to a carrier thermal ionization process. No significant changes in the line widths of both RBM and the G-band as well as vanishing or insignificant D-band suggest mild noncovalent functionalization in charge transfer doping of semiconducting SWNTs with PEI. Very different spectral responses in metallic SWNTs (namely, the appearance of Fano line shape and the concurrent enhancement of D-band) have important implications on the intrinsic phonon line shape and therefore on the electron−phonon coupling. In particular, we have experimentally shown that at least certain metallic tubes exhibit symmetric Lorentzian line shapes for the G-band phonon mode and that the changes in the local chemical environment can lead to the appearance of Fano line shape with associated enhancement of the D-mode even in the *isolated* (unbundled) metallic SWNTs.

Acknowledgment. This work was supported by the NSF (Grant Nos. DMR-0348585 and CCF-0506660). We made use of the facilities at the Center for Microanalysis of Materials, University of Illinois, which is partially supported by the U.S. Department of Energy under Grant No. DEFG02-91-ER45439.

Supporting Information Available: Tentative assignment of chiral indices (n, m) for the semiconducting carbon nantoubes shown in Figure 4. This material is available free of charge via the Internet at http://pubs.acs.org.

JA058551I